Low-Profile Dual-Polarized Antenna Loaded With Electromagnetic Band-Gap Structures

Nallagundla Suresh Babu[1] [ID] **· Abdul Quaiyum Ansari[1] · Deepak Gangwar[2] · Binod Kumar Kanaujia[3] · Sachin Kumar[4] · Surendra Kumar Gupta[5]**

Abstract

In this work, a dual-band dual circularly polarized coplanar waveguide (CPW)-fed monopole antenna is presented. The antenna consists of the modified ground plane, and two rectangular-shaped radiators, which are located on the two sides of the monopole. The radiating patches are loaded with metamaterial dependent electromagnetic band-gap structures for obtaining wider impedance bandwidth and broad axial ratio characteristics. The proposed antenna features impedance bandwidth of 97.4% (1–2.9 GHz) in the first band and 61.36% (3.05–5.75 GHz) in the second band, covering applications of ISM-band (2.4–2.48 GHz), Wi-MAX (2.5–2.69 GHz, 3.4–3.69 GHz), and WLAN (2.4–2.48 GHz, 5.15–5.35 GHz). The antenna also features dual circular polarization with 3-dB axial ratio bandwidth of 33.8% (1.35–1.9 GHz) and 35.7% (3.1–4.45 GHz), in the first and second bands, respectively. The first band shows right-hand circular polarization, whereas the second band exhibits left-hand circular polarization.

✉ Nallagundla Suresh Babu
  sureshjmiphd@gmail.com

  Deepak Gangwar
  deepak.gangwar@mjpru.ac.in

  Sachin Kumar
  gupta.sachin0708@gmail.com

[1] Department of Electrical Engineering, Faculty of Engineering and Technology, Jamia Millia Islamia, New Delhi 110025, India

[2] Department of Electronics and Instrumentation Engineering, Mahatma Jyotiba Phule Rohilkhand University, Bareilly 243006, India

[3] Department of Electronics and Communication Engineering, Dr. B. R. Ambedkar National Institute of Technology Jalandhar, Jalandhar 144027, India

[4] Department of Electronics and Communication Engineering, Galgotias College of Engineering and Technology, Greater Noida 201310, India

[5] Department of Electronics Engineering, Ambedkar Delhi Skill and Entrepreneurship University Campus Shakarpur–I, Delhi 110092, India

1 Introduction

Recently, the electromagnetic band-gap (EBG)-based patch antennas are receiving significant attention of the researchers, as they prevent the propagation of unwanted surface-waves (within a specific frequency band) and zero-phase reflection of the incident plane wave. These two features enable a researcher to design compact antennas, without compromising the antenna radiation performance. EBG was first investigated by E Yablonovitch and S. John, in 1987 [1], as a periodic arrangement of metal patches [2]. Usually, the EBG structures are printed on the ground plane, and they are short-circuited through the metal patches and the ground plane. High impedance surface (HIS) is a type of EBG structure, without any short circuit connection between the metal patches and the ground plane [3–6]. A microstrip patch antenna with small size, simple fabrication without any vias, and dual-band characteristics was presented in [3]. In [4], the EBG surface performed like a periodically loaded capacitor or inductor, which, in turn, used as a band-pass filter. In [5], using Fabry–Perot (FP) cavity antenna, the dielectric phase correcting structures were designed to increase gain, directivity, aperture efficiency, and reduce side lobes levels. A compact-sized EBG structure for millimetre-waves was reported in [6]. It showed wide band-gap of around 60 GHz, reduction in the size of the unit cell, and mutual coupling reduction in the antenna arrays. In [7], the reflection phase characteristic of the mushroom-like EBG structure was presented, where the EBG was used to change polarization (linearly to circularly) of the incident wave. A 3-dB axial ratio bandwidth (ARBW) of 19.9% (2.81–3.43 GHz) was achieved. Likewise, in [8], a low-profile linearly polarized dipole antenna features impedance bandwidth of 24% (3.25–4.14 GHz) and ARBW of 5.6% (3.45–3.65 GHz). Introduction of a diagonally placed slot at a slanting of 45° in a square like metallic patch embedded on metamaterial substrate for producing circular polarization was reported in Ref. [9], with impedance bandwidth of 14% (2.08–2.4 GHz) and ARBW of 10.6% (2.179–2.42 GHz). A circularly polarized patch antenna composed of artificial ground structure with rectangular unit cells was presented in Ref. [10], where impedance bandwidth of 48.6% (4.52–7.52 GHz) and ARBW of 20.4% (5.4–6.63 GHz) was reported. A dual-mode patch antenna based on EBG structure was proposed in Ref. [11], the antenna resonates at 1.34 GHz, 1.91 GHz, and 2.38 GHz, and illustrated ARBW of 1% (2.375–2.4 GHz). A compact self-polarizing FP cavity antenna was presented in [12], which can change linear polarization (at 45°) to circular polarization. It showed an impedance bandwidth of 1.12% (2.49–2.52 GHz) and ARBW of 1.9% (2.51–2.56 GHz).

Introduction of a transversely located slot at an inclination of 42° on the ground surface and supported by an array of rectangular formed metallic unit cells for producing circular polarization was presented in [13], with an impedance bandwidth of 33.7% (4.20–5.90 GHz) and ARBW of 16.5% (4.90–5.90 GHz). Loading of a slot with slanting of 53° and supported by U-shaped slotted rectangular EBG array for generating circular polarization was demonstrated in [14], with impedance bandwidth of 34.6% (2.82–4 GHz) and ARBW of 6.8% (3.135–3.354 GHz). A circular ring-shaped slot antenna with EBG structure was proposed for wireless body wearable applications [15], which showed an impedance bandwidth of 14.63% (2.28–2.64 GHz) and the front-to-back ratio (FBR) of 17 dB. An antenna with a curtailed square patch and supported by rectangular slotted circular like EBG metasurface was proposed in Ref. [16], with an impedance bandwidth of 37% (5.07–7.3 GHz) and ARBW of 5.9% (5.24–5.56 GHz). A patch array with compact EBG structure was presented in Ref. [17], which showed an impedance bandwidth of 3.03% (5.51–5.68 GHz). A two-element multiple-input-multiple-output (MIMO)

antenna with fractal-formed EBG array to minimize the mutual coupling was reported, with an impedance bandwidth of 5.04% (5.8–6.1 GHz) [18]. A compact size broadband antenna with EBG structures was proposed in Ref. [19], offers an impedance bandwidth of 24.4% (2.67–3.412 GHz). A MIMO antenna with small size uniplanar EBG was proposed for broadband characteristics [20], which achieves an impedance bandwidth of 133% (3.6–17.9 GHz). Carving out of a 45° turn round rectangular like slot in the middle of a radiating element with EBG for generating circular polarization was reported in Ref. [21]. It showed an impedance bandwidth of 5.3% (2.349–2.477 GH) and ARBW of 1.23% (2.4269–2.477 GHz). A microstrip monopole antenna composed of uniplanar compact EBG structure was proposed in Ref. [22], where impedance bandwidth of 16% (2.3–2.7 GHz) and cross-polarization suppression was achieved. However, the above-reported antennas with EBG are difficult to manufacture due to their multi-layered and via holes geometry, large size and weight, and limited ARBW.

A rectangular-like patch with truncated slots and defected surface, loaded with engraved circular like EBG configuration, was presented in Ref. [23]. It demonstrated an impedance bandwidth of 73.29% (4.97–10.72 GHz) and ARBW of 13.66% (7.5–8.6 GHz). An english alphabet T-like radiating patch loaded with EBG configuration was presented in Ref. [24], which showed an impedance bandwidth of 2.09% (3.496–3.57 GHz). A circularly polarized antenna with slanting feeding in a rectangular like radiating patch, slotted ground surface, and rectangular ring metasurface unit cells was presented in Ref. [25]. It showed first impedance bandwidth of 3.17% (1.55–1.6 GHz), second impedance bandwidth of 2.6% (2.3–2.36 GHz), and ARBW of 3.17% (1.55–1.6 GHz).

In this paper, a coplanar waveguide (CPW)-fed dual-band dual circularly polarized monopole antenna with EBG structure-dependent metamaterial is presented. The antenna consists of a monopole and two rectangular-shaped radiating elements located on each side of the monopole. The two rectangular patches are loaded with EBG structures. In the antenna, an inverted U-shaped stub and a quasi-C-shaped open-loop stub are introduced to achieve wider axial ratio and impedance bandwidths. The measured results show that impedance bandwidths of 97.4% (1–2.9 GHz) and 61.36% (3.05–5.75 GHz) are obtained in the first and second bands, respectively. In the first band, 3-dB ARBW of 33.8% (1.35–1.9 GHz) is achieved, whereas, in the second band, the ARBW is 37.9% (3.1–4.55 GHz). The lower band shows RHCP, while the upper band exhibits LHCP behaviour.

The paper is organized as follows: Sect. 2 describes the EBG metamaterial unit cell and its band-gap characteristics. The evolution of the proposed antenna is presented in the Sect. 3. The antenna layout and results are explained in Sect. 4, and a conclusion is presented in Sect. 5.

2 Characterization of the EBG Metamaterial Unit Cell

Metamaterials are synthetic crafted materials with unique electromagnetic traits, portrayed by unit cells much lower than the wavelength of incident radiation. Metamaterials display attributes of backward-wave transmission, yielding a negative refractive index, as originally theorized by V. Veselago [26]. Early implementation of such negative refractive index concept employing large sized periodic arrays of fine wires and split ring resonators [27]. The two-dimensional metamaterial EBG structure detailed in Ref. [28] was attained through the periodic loading of a planar network of imprinted transmission lines with series connecting capacitors and shunt connected inductors structured in a twin-transmission lines

(high-pass) arrangement. A metamaterial-built EBG configuration proposed in Ref. [29] was composed of interdigitated capacitive conductive elements along with stub inductive bridged elements backed by ground surface for generating a bandgap of 4.3–6.8 GHz. A miniaturized EBG configuration was reported in Ref. [30], with series connected inter-digitized capacitances and shunt connected stub inductances, for obtaining a bandgap from 2.4 to 6 GHz. In [31], three resonances at frequencies of 2.4 GHz, 3.6 GHz, and 5 GHz were achieved by integrating two different sections of metamaterial-formed EBG structures. An EBG configuration was composed of amalgamating interdigitated series elements along with rectangular like slits in Ref. [32]. This configuration exhibits a broad bandgap from 3.4 to 6.2 GHz, but it is unable to provide resonance at 2.4 GHz. An EBG configuration along with loading of interdigitated conducting capacitor elements to obtain a bandgap from 1.5 to 3.5 GHz was presented in Ref. [33].

EBG structures are artificially created periodic arrangements that either facilitate or impede the propagation of electromagnetic waves across a specified spectrum, regardless of incident angles or polarization modes. These structures typically consist of metallic stubs or slotted conducting/insulating materials. One of the key advantages of EBG configurations lies in their capability to mitigate the impact of surface wave current. Surface waves tend to degrade antenna performance by reducing gain and efficiency, increasing cross-polarization and end-fire radiation, and fostering overall poor antenna performance [34, 35]. Furthermore, surface waves improve coupling between adjoining antenna elements within an antenna array. However, combining of EBG configurations with the antenna/filter helps in suppressing surface waves, thereby enhancing antenna functionality by elevating gain and reducing backward radiations [36].

A study presented in Ref. [37] introduced an EBG array possessing mushroom-like elements, comprising of a ground surface, metallic stub patches, and shorted metallic vias. This EBG array configuration demonstrated stop band attributes, effectively preventing the propagation of surface waves. The functionality of the EBG configuration was elucidated using an *LC* equivalent circuit, serving as an electrical stop band filter to inhibit surface wave propagation [38]. The flow of current through the shorted vias results in the generation of the inductor (*L*), while the gap between adjoining patches yields the capacitor (*C*). The values of inductor and capacitor for an EBG configuration, with parameters such as patch width (*W*), gap width (*g*), substrate thickness (*h*), and dielectric constant (ε_r), can be computed using Eqs. (1)–(4) [39].

$$L = \mu_0 h \tag{1}$$

$$C = \frac{W\varepsilon_0\left(1 + \varepsilon_0\right)}{\pi}\cosh\frac{(2W + g)}{g} \tag{2}$$

In free space, the permeability (μ_0) and permittivity (ε_0) are given as,

$$\omega = \frac{1}{\sqrt{LC}} \tag{3}$$

$$BW = \frac{\Delta\omega}{\omega} = \frac{1}{\eta}\sqrt{\frac{L}{C}} \tag{4}$$

The layout of the unit cell is shown in Fig. 1a and b. The unit cell is printed on FR-4 epoxy substrate (relative permittivity = 4.4 and loss tangent = 0.024) of dimensions $W_U \times L_U \times h$. ANSYS HFSS tool is used to perform the simulations of the proposed unit cell and the antenna. The working of an EBG unit cell can be explained by an LC equivalent circuit, whose time period is small as compared to the operating wavelength [40]. As shown in Fig. 1a and b, the inductor (L) is established by the rectangular-shaped conductor strips, and capacitance (C) is established by the spacing between the two neighbouring strips. The band-gap characteristics are dependent on the permittivity, dimensions, and periodicity of the substrate material [41]. The dispersion diagram of the EBG unit cell is shown in Fig. 1c, where the surface wave phase variations from Γ to X, X to M, and M to Γ (called Brillouin zone) for mode 1 and mode 2 are presented. The distance between mode 1 and mode 2 is called the bandgap region, which is about 1.1 GHz (2.7–3.8 GHz) in the proposed unit cell.
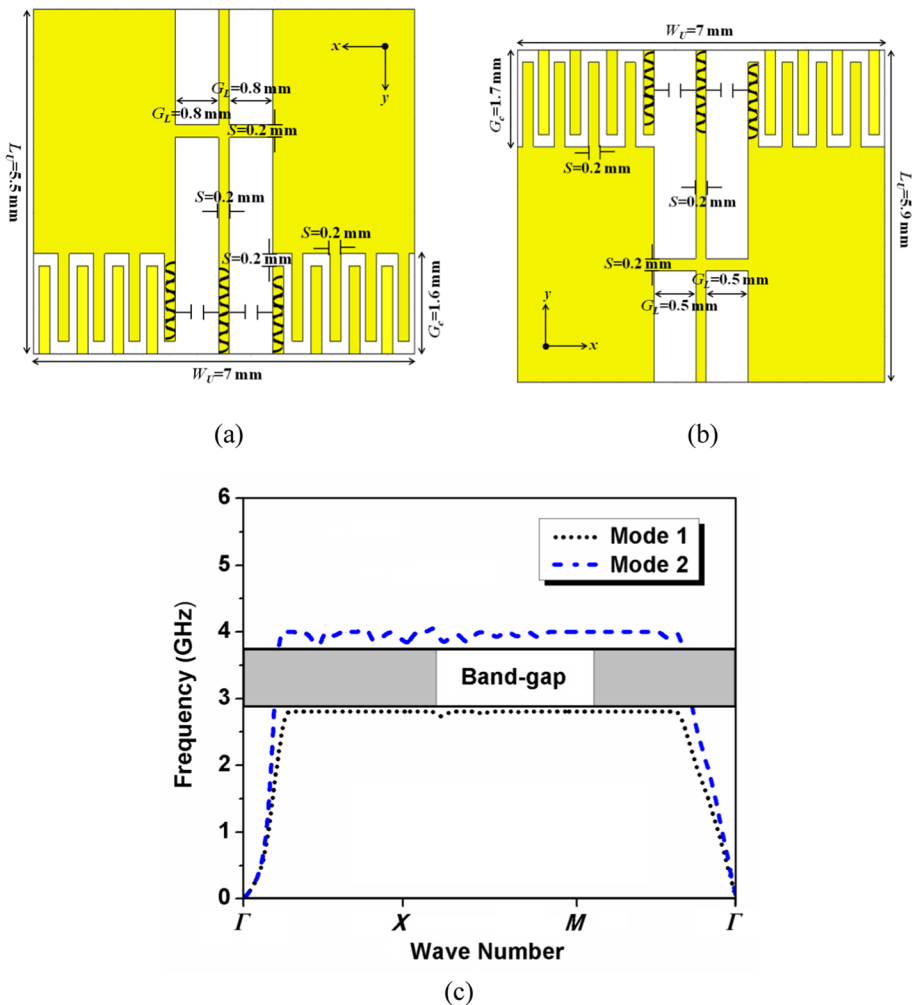

Fig. 1 Metamaterial unit cell: **a** feed-sided, **b** front-sided, **c** dispersion diagram

The proposed radiating patch is presented in Fig. 2a, which consists of five EBG unit cells. Out of five, three unit cells (shown in Fig. 1b) are printed at the lower edge of the antenna, and two unit cells (shown in Fig. 1a) are printed at the top side of the antenna. The proposed EBG-based radiator, which is printed on the FR-4 epoxy substrate, acts as a parasitic element in the proposed antenna. The return loss and axial ratio characteristics of the radiating patch are illustrated in Fig. 2b. The radiator shows linearly polarized behaviour at frequencies 2.4 and 5 GHz.

3 Evolution of the Proposed Antenna

The design steps of the proposed CPW-fed antenna are illustrated in Fig. 3a–h. The corresponding return loss and axial ratio characteristics are compared in Fig. 4a–d. Initially, a traditional rectangular like CPW-fed monopole antenna 1 is designed, as shown in Fig. 3a, which produces the resonant mode at 0.9 GHz with an impedance bandwidth of 38.2% (0.72–1.06 GHz). The hybrid mode principal resonance frequency is estimated by Ref. [42, 43],

$$L_{res} = 2L_{Ebg1} + W_{Ebg1} + 2\Delta l_{eff} \tag{5}$$

where the fringe field depth Δl_{eff} is equivalent to the substrate thickness ($h = 1.6$ mm), $L_{Ebg1} = 28.2$ mm and $W_{Ebg1} = 21$ mm are the length and width of the conventional rectangular formed CPW-fed monopole antenna 1, respectively. The length of conventional rectangular monopole CPW-fed antenna is ($L_{res} = 80.6$ mm), and the principal resonance frequency is calculated as,

$$f_r = \frac{c}{2L_{res}\sqrt{\varepsilon_r}} \tag{6}$$

where ε_r is the dielectric constant of the substrate material. It displays that the traditional CPW-built rectangular formed monopole antenna 1 generates impedance bandwidth
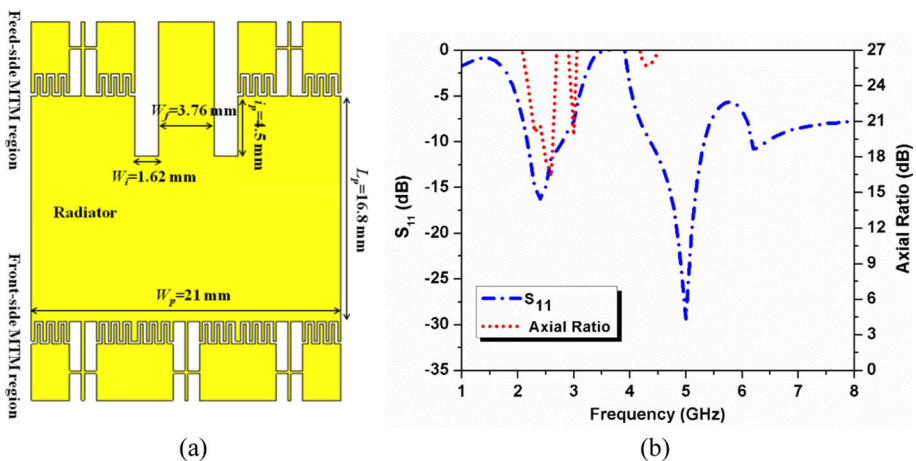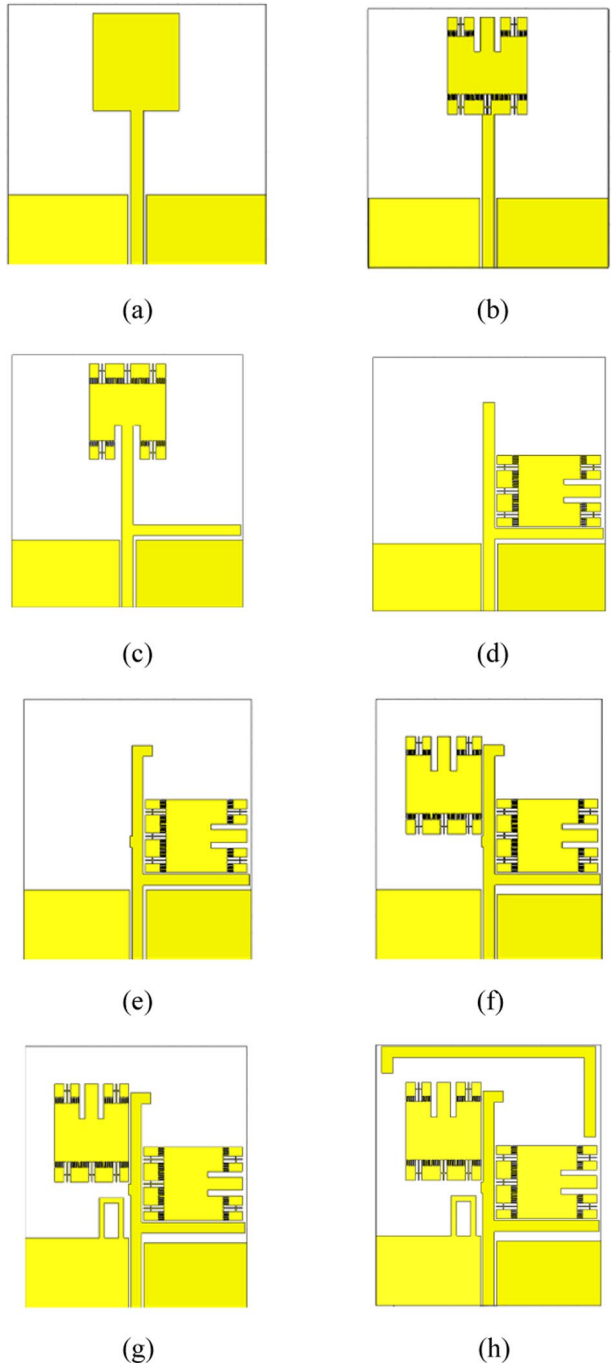

Fig. 2 Radiating element of the proposed antenna: **a** schematic, **b** simulated return loss and axial ratio characteristics

Fig. 3 EBG-based proposed monopole antenna: **a** antenna 1, **b** antenna 2, **c** antenna 3, **d** antenna 4, **e** antenna 5, **f** antenna 6, **g** antenna 7, **h** antenna 8
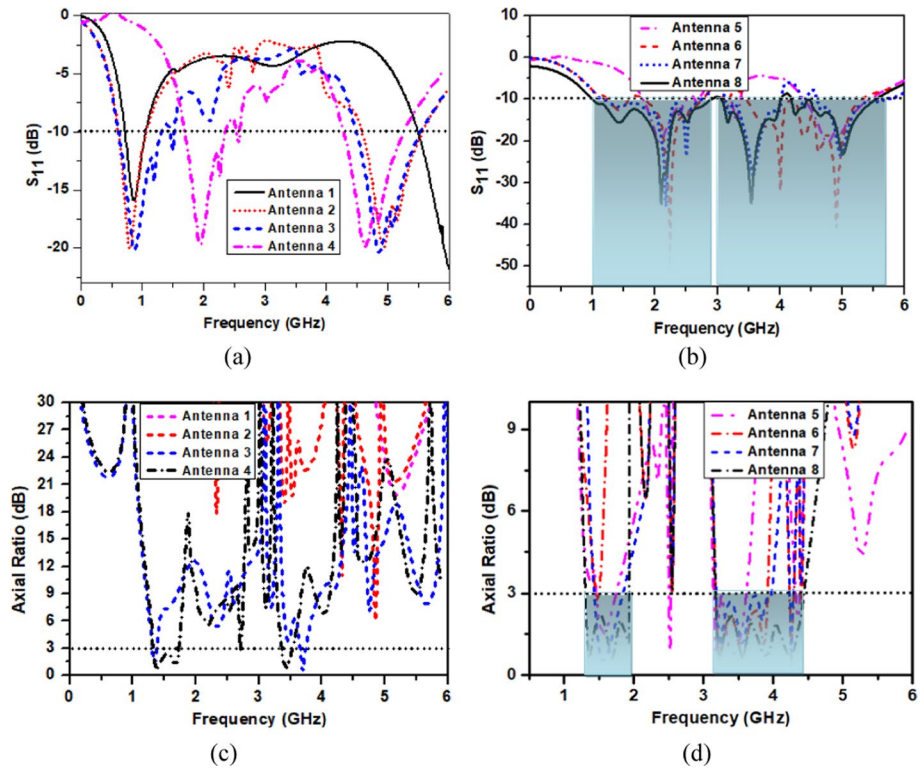

(a)

(b)

(c)

(d)

(e)

(f)

(g)

(h)

Fig. 4 EBG MTL-based antenna design steps comparison: **a** return loss for antenna 1–4, **b** return loss for antenna 5–8, **c** axial ratio for antenna 1–4, **d** axial ratio for antenna 5–8

(− 10 dB) of 38.2% (0.72–1.06 GHz) with resonance frequency at 0.9 GHz and it is substantiated with simulated resonant frequency of 0.9 GHz, as shown in Fig. 4a.

Achieving circular polarization in the conventional monopole antenna 1 is very challenging due to the radiation cancellation in horizontal direction, as shown in Fig. 5a and b. It is observed that the surface current distributions propagating along the two pairs of ground planes in antenna 1 at (0.9 and 1.05 GHz) are equal in magnitude and opposite in phase. Hence, the radiation in the horizontal direction along the two pairs of ground planes are cancelled as they are opposite in direction. Therefore, antenna 1 generates linear polarization, as displayed in Fig. 4c.

In order to generate a second resonance, an EBG-based patch is inserted in place of traditional rectangular antenna 1, shown in Fig. 3a, which resonates at 0.9 and 5 GHz and it is validated with reflection coefficients displayed in Fig. 2b. From Fig. 5c and d, it is observed that the surface current distributions along the ground plane (at frequencies 0.9 and 5.07 GHz) are equal in magnitude and opposite in phase. Since the current vectors are in opposite direction, the radiation in the horizontal direction gets cancel out. Therefore, the antenna 2 generates linearly polarized waves and it obtains − 10 dB impedance bandwidth improvements of 54.1% (0.62–1.08 GHz) at lower band and at higher band it generates 19.3% (4.58–5.56 GHz), as depicted in Fig. 4a. For circular polarization, the electric field of a plane wave must have two orthogonal components with equal magnitude and
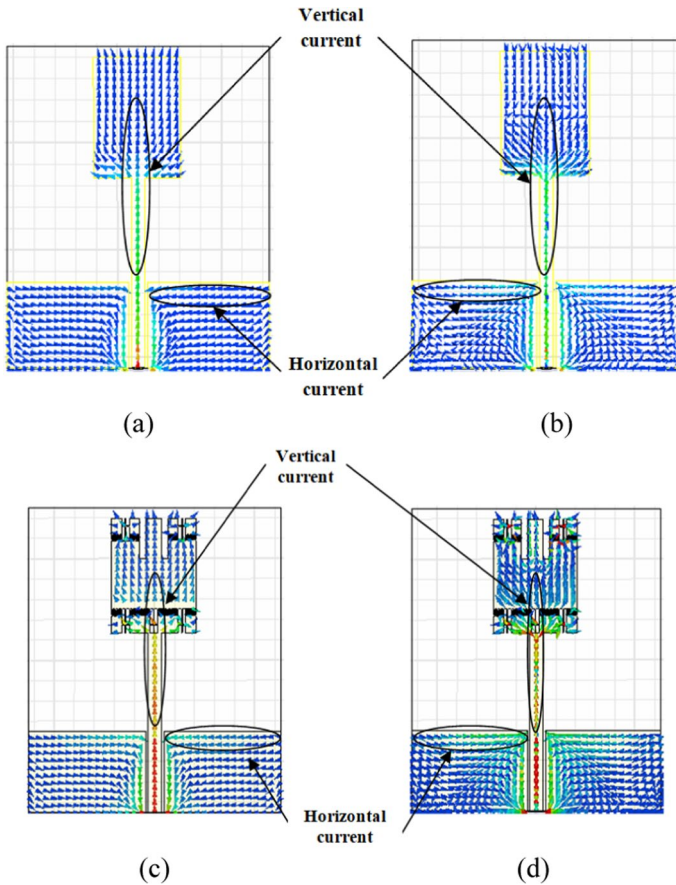
Fig. 5 Simulated surface current distribution at **a** 0.9 GHz, **b** 1.05 GHz, **c** 0.9 GHz, **d** 5 GHz

90° out of phase. Therefore, the technique of achieving circular polarization by introducing stub/strip in [44, 45] is implemented in antenna 3. Figure 3b is joined to the horizontal rectangular strip/stub to achieve two electric field orthogonal components. In antenna 3, as shown in Fig. 3(c), circular polarization is obtained at 1.35 GHz (1.3–1.39 GHz) and at 3.7 GHz (3.6–3.8 GHz). The corresponding impedance bandwidths are 60.9% (0.65–1.22 GHz) and 20% (4.5–5.5 GHz).

To achieve the new resonant frequency of 2 GHz, the EBG structure located vertically in Fig. 3c is shifted and placed just above the rectangular horizontal line (with a gap of 0.5 mm) (antenna 4), as shown in Fig. 3d. The shifting of frequency from lower band of 0.9 GHz to higher band of 2 GHz is due to the reduction in length of the antenna (by shifting the EBG metamaterial structure). The antenna 4 exhibits impedance bandwidth of 63.4% (1.4–2.7 GHz) at 2.05 GHz and 28% (4.3–5.7 GHz) at 5 GHz. It also offers larger 3-dB ARBW of 11.3% (1.25–1.4 GHz) and 9.9% (3.35–3.7 GHz). For generating a new resonant frequency, additional metallic strips/stubs are introduced in the presented antenna design [46, 47]. A horizontal rectangular strip of length 0.5 mm and width of 3.2 mm, and a rectangular strip of length 5.7 mm and width of 3.2 mm, are integrated in the left

side and top of a vertical rectangular-like monopole antenna [48], resulting in antenna configuration 5, as shown in Fig. 3e. It achieves enhancement in impedance bandwidth with 67.3% (1.25–2.72 GHz) and 40.9% (3.4–5.15 GHz). Also, it obtains 3-dB ARBW of 15.4% (1.5–1.75 GHz) and 16.6% (3.3–3.9 GHz), as illustrated in Fig. 4d.

In antenna 6, as shown in Fig. 3f, a second EBG configuration acting as a parasitic element is introduced in the left side of the rectangular monopole antenna for bandwidth enhancement [49, 50]. A further bandwidth improvement is achieved by making the right sided ground surface asymmetrical with a shorter length (20–18.5 mm) in comparison to the left sided ground surface [51, 52], as shown in Fig. 6b. Figure 3f shows that antenna 6 increases impedance bandwidth by 83.5% (1.13–2.75 GHz) and 43.3% (3.35–5.2 GHz). It also improves 3-dB ARBW by 21.5% (1.45–1.8 GH) and 23.4% (3.25–4.1 GHz), as shown in Fig. 4d.

To achieve impedance matching in the proposed antenna, an inverted U-shaped stub (of dimensions 11.5 mm×6.95 mm) is introduced at a distance of 1.9 mm from the vertical radiator (antenna 7) [46], as shown in Fig. 3g. The antenna 7 shows 3-dB ARBW of 27.6% (1.45–1.85) GHz and 29.3% (3.2–4.3 GHz). Also, it demonstrates enhancement in impedance bandwidths of 88.6% (1.08–2.8 GHz) and 53.9% (3.14–5.46 GHz), as displayed in Fig. 4d. The final antenna design is obtained by introducing an inverted quasi-C shaped open loop stub in the upper surface [53–56], which covers the upper portion of the antenna, as shown in Fig. 3h. The stub is capacitively coupled by the below located vertical monopole radiator due to the electromagnetic interaction between them. Therefore, the inverted
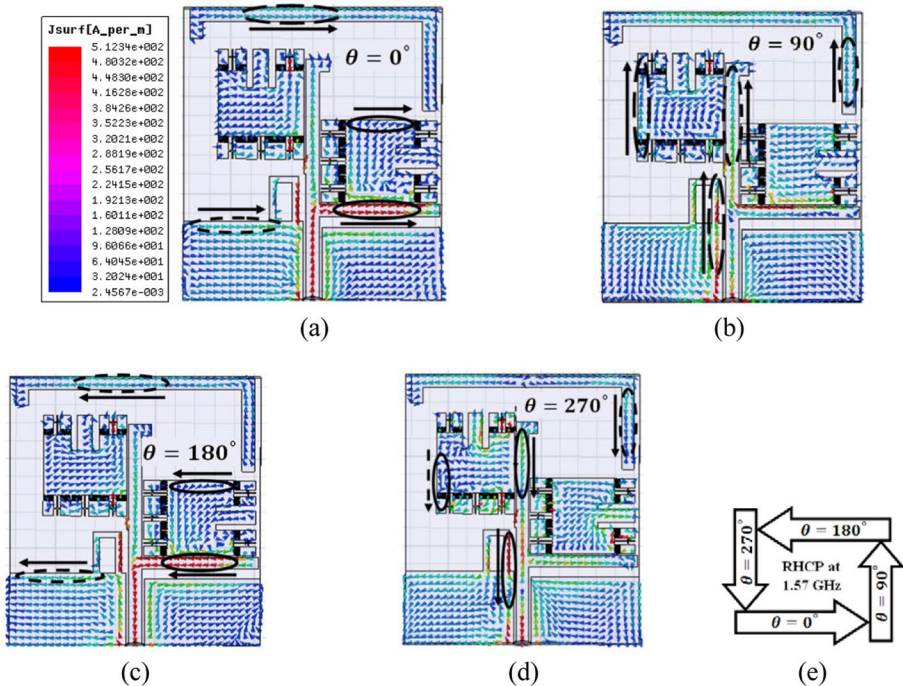

Fig. 6 Surface current distribution of the proposed antenna at 1.57 GHz: **a** 0°, **b** 90°, **c** 180°, **d** 270°, **e** direction of current (RHCP)

C-shaped metallic stub behaves like a parasitic stub, which is able to transmit the radiated power after receiving the radiated power from the antenna, and this leads to dual-mode 10-dB return-loss bandwidths of 97.4% (1–2.9 GHz) and 61.36% (3.05–5.75 GHz). Further, it features 3-dB ARBW of 33.8% (1.35–1.9 GHz) and 35.7% (3.1–4.45 GHz). Table 1 displays the improvement in the performance attributes in evolution of the proposed antenna.

Figure 6 shows surface wave current distribution of the proposed EBG-based CPW-fed monopole antenna at frequency 1.57 GHz for phases 0°, 90°, 180°, and 270°. It is observed from Fig. 6a that at 0°, the surface current direction is primarily in + y-direction. At 90°, the direction of the current is mainly in –x-direction, as shown in Fig. 6b. At 180° and 270°, shown in Fig. 6c and d, the direction of the current is in –y-direction and + x-direction, respectively. Since the current is rotating in an anti-clockwise direction, as displayed in Fig. 6e, hence, RHCP is obtained.

Similarly, the surface current distribution at frequency 3.65 GHz for phases 0°, 90°, 180°, and 270° is depicted in Fig. 7. It is observed from Fig. 7a that at 0°, the direction of surface current is primarily in + x-direction. At 90°, as shown in Fig. 7b, the direction of the current is mainly in –y-direction. At 180° and 270° phases, shown in Fig. 7c and d, the direction of current is in –x-direction and + y-direction, respectively. Since the current is rotating in a clockwise direction as shown in Fig. 7e, hence, LHCP is obtained. Figure 8 also verifies the RHCP and LHCP patterns at 1.57 and 3.65 GHz, respectively.

4 Results and Discussion

The geometry of the proposed CPW-fed monopole antenna is illustrated in Fig. 9a. The dimensions of the design parameters are shown in Table 2. The monopole antenna consists of two EBG metamaterial-based parasitic elements, inverted quasi-C-shaped open-loop stub, and inverted U-shaped stub integrated with the partial ground plane. The overall size of the proposed CPW-fed antenna is $W \times L \times h$ (63 mm × 75 mm × 1.6 mm). The fabricated prototype of the CPW-fed monopole antenna is shown in Fig. 9b. The prototype of the proposed antenna in an anechoic chamber is shown in Fig. 9c, and its experimental measurement is shown in Fig. 9d.

Two EBG metamaterial-based radiators (shown in Fig. 2a), located horizontally and vertically, are used as parasitic elements in the proposed monopole antenna. The distance between the parasitically coupled radiators and the feed line is 0.5 mm. A parasitic element is a tuned circuit, which does not have its own feeding and is dependent on some other system. In the proposed antenna, the radiated energy from the monopole is coupled to the EBG-based radiators, which, in turn, sets up a magnetic field. The magnitude and phase of the induced voltage depend on the length of the parasitic element, and spacing between the feeder and driven element. Furthermore, an inverted C-shaped open-loop slot is introduced at the top of the antenna to improve −10 dB impedance bandwidth and 3-dB ARBW.

Figure 10 shows the simulated and measured return loss and axial ratio characteristics of the proposed EBG metamaterial-based CPW-fed monopole antenna. It is noticed from Fig. 10a that the antenna provides dual-band performance with measured impedance bandwidths of 76.54% (1.25–2.8 GHz) and 61.36% (3.05–5.75 GHz). Further, the measured and simulated axial ratio performance characteristics are shown in Fig. 10b. The measured ARBWs in the two bands are 28.57% (1.35–1.8 GHz) (RHCP) and 37.9% (3.1–4.55 GHz) (LHCP). The simulated results are in agreement with the measured results, except a little variation in the second band, which is due to fabrication tolerance.

Table 1 Performance attributes of the proposed antenna evolution

| Antenna type	Impedance bandwidth (in%)	Impedance bandwidth (in%)	Axial ratio bandwidth (in%)	Axial ratio bandwidth (in%)
Antenna 1	38.2 (0.72–1.06 GHz)	—	—	—
Antenna 2	54.1 (0.62–1.08 GHz)	19.3 (4.58–5.56 GHz)	—	—
Antenna 3	60.9 (0.65–1.22 GHz)	20 (4.5–5.5 GHz)	6.7 (1.3–1.39 GHz)	5.4 (3.6–3.8 GHz)
Antenna 4	63.4 (1.4–2.7 GHz)	28 (4.3–5.7)	11.3 (1.25–1.4 GHz)	9.9 (3.35–3.7 GHz)
Antenna 5	67.3 (1.25–2.72 GHz)	40.9 (3.4–5.15 GHz)	15.4 (1.5–1.75 GHz)	16.6 (3.3–3.9 GHz)
Antenna 6	80.4 (1.13–2.75 GHz)	43.3 (3.35–5.2 GHz)	21.5 (1.45–1.8 GHz)	23.4 (3.25–4.1 GHz)
Antenna 7	87.2 (1.08–2.8 GHz)	53.9 (3.14–5.46 GHz)	27.6 (1.45–1.85)	29.3 (3.2–4.3 GHz)
Antenna 8	97.4 (1–2.9 GHz)	61.36 (3.05–5.75 GHz)	33.8 (1.35–1.9 GHz)	35.7 (3.1–4.45 GHz)
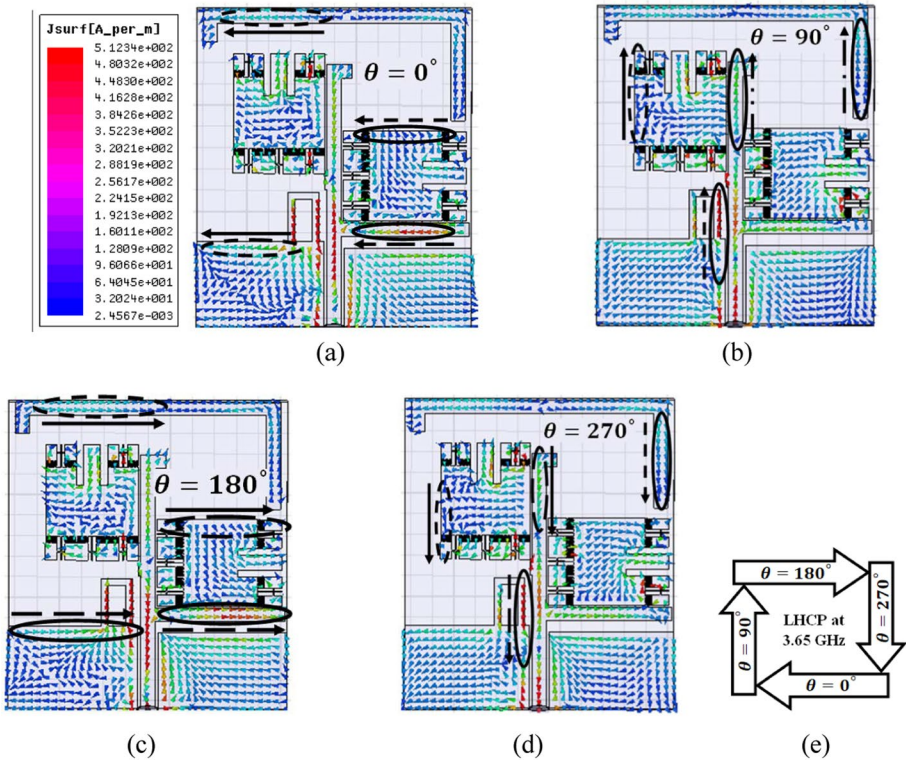
Fig. 7 Surface current distribution of the proposed antenna at 3.65 GHz: **a** 0°, **b** 90°, **c** 180°, **d** 270°, **e** direction of current (LHCP)

Fig. 8 Circular polarization characteristics at frequencies 1.57 GHz (RHCP) and 3.65 GHz (LHCP)
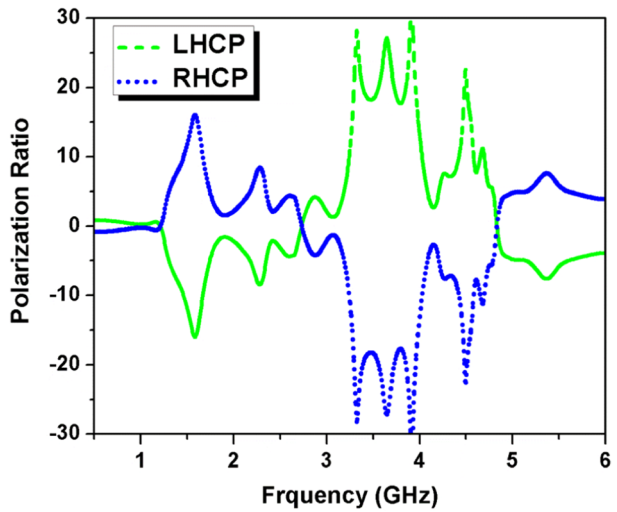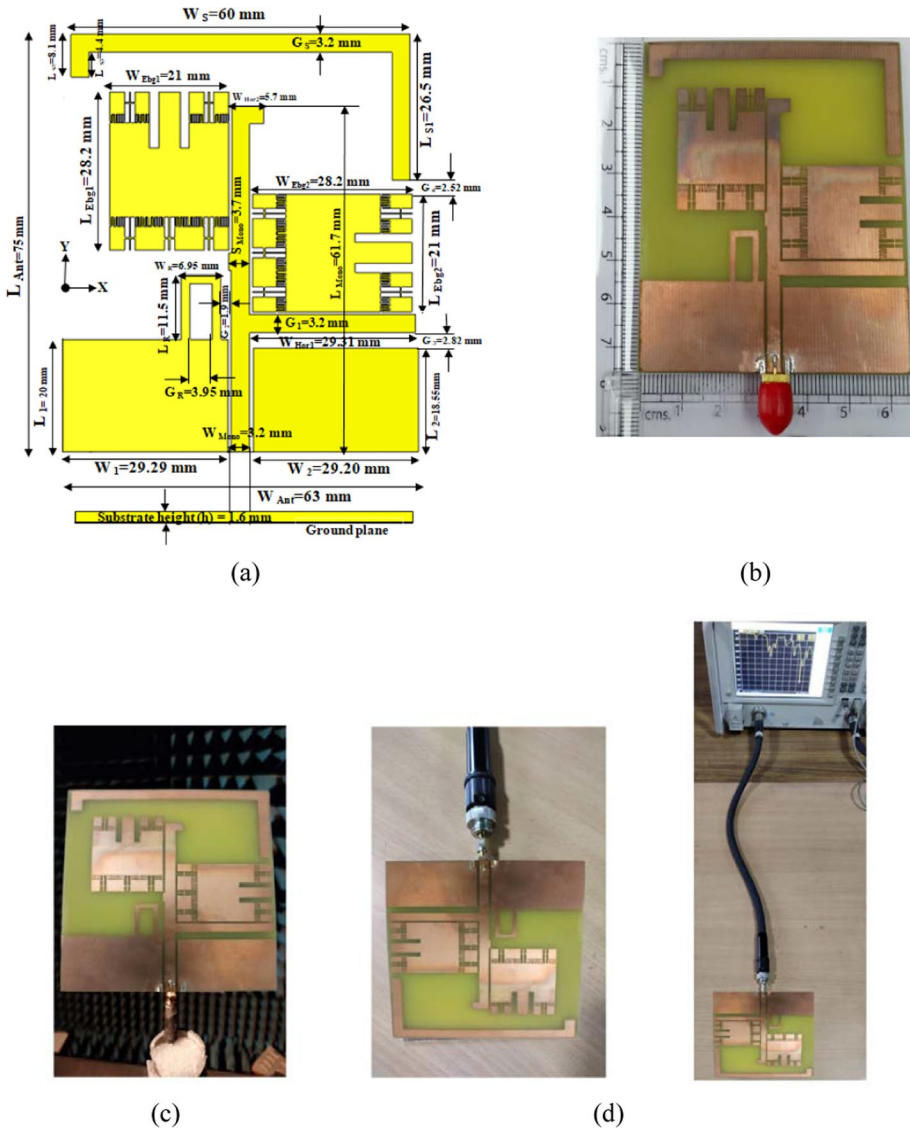
Fig. 9 Proposed CPW-fed monopole antenna: **a** layout, **b** fabricated prototype, **c** in an anechoic chamber, **d** measurement

The simulated and measured gain plots of the designed EBG-based CPW-fed antenna are shown in Fig. 11a. The simulated gain varies from 1.1 to 4 dB and measured gain varies from 0.8 to 3.7 dB. Table 1 shows that the proposed antenna design improves its impedance bandwidth and ARBW only by including additional strip/stub elements. Furthermore, Fig. 11b shows a comparison of gain with and without adding stub elements, and it is clear that the gain only increases when additional stub elements are added to

Table 2 Design values of the EBG MTM-based CPW-fed monopole antenna

| Parameter	Dimensions (mm)	Parameter	Dimension (mm)	Parameter	Dimension (mm)	Parameter	Dimension (mm)
L_{Ant}	75	L_1	20	G_3	2.82	L_{S2}	8.1
W_{Ant}	63	W_1	29.29	G_4	2.52	L_{s3}	4.4
L_{Mono}	61.7	L_2	18.55	L_{Ebg1}	28.2	G_S	3.2
W_{Mono}	3.2	W_2	29.20	W_{EBG1}	21		
S_{Mono}	3.7	L_R	11.5	L_{EBG2}	21		
W_{Hor1}	29.31	W_R	6.95	W_{EBG2}	28.2		
W_{Hor2}	5.7	G_R	3.95	W_S	60		
G_1	3.2	G_2	1.9	L_{S1}	26.5		

the antenna. The simulated efficiency varies from 75 to 96.5%, as shown in Fig. 11c, and measured efficiency varies from 71.5 to 92.5%.

Figure 12 shows the simulated and measured radiation patterns (in XOZ-plane and YOZ-plane) of the EBG-based CPW-fed antenna at frequencies 1.45 GHz, 3.63 GHz, and 4.34 GHz. The cross-polarization level is 15 dB down with respect to the direction of maximum radiation. The EBG-based monopole antenna radiates RHCP waves at 1.45 GHz and LHCP waves at 3.63 and 4.34 GHz.

Table 3 presents a comparison of the proposed EBG-based CPW-fed circularly polarized monopole antenna with other EBG-based antennas [7–25] reported in the literature. The proposed antenna offers several advantages over these reported designs, including dual-band operation, lower antenna height, smaller number of unit cells, superior radiation efficiency, simple geometry without any via holes, compact size, light weight, and easily integrable with microwave integrated circuits (MICs) due to its uniplanar design. The key advantages of the designed antenna are as follows:

- In comparison to other communicated EBG-built single band antennas [7–25], the proposed antenna provides dual resonating bands, and a broader impedance bandwidth and larger ARBW.
- Unlike the previously reported antennas [7–25], the proposed antenna offers dual circular polarization, which encounters the fading effect and polarization mismatch losses.
- In contrast to other reported EBG-formed antenna structures [7–16, 19] and [21–25], the suggested antenna has smaller antenna height. Also, the proposed antenna requires a smaller number of EBG unit cells.
- Unlike the previously reported EBG-based antennas [8–16, 19, 21–25], the presented antenna offers single layered configuration. Though the antennas in [17, 18, and 20] showed single layer, but they need more antenna elements due to MIMO configuration and requires complicated slotted EBG structures with shorted vias.
- The presented antenna provides greater radiation efficiency in contrast to other reported antenna configurations [7–25].
- The proposed antenna operates at the widely used ISM (2.4–2.48 GHz) and WLAN bands (2.4–2.48 GHz and 5.15–5.35 GHz). Also, the presented antenna achieves a

Fig. 10 Simulated and measured results of the EBG-based CPW-fed monopole antenna: **a** S_{11}, **b** axial ratio
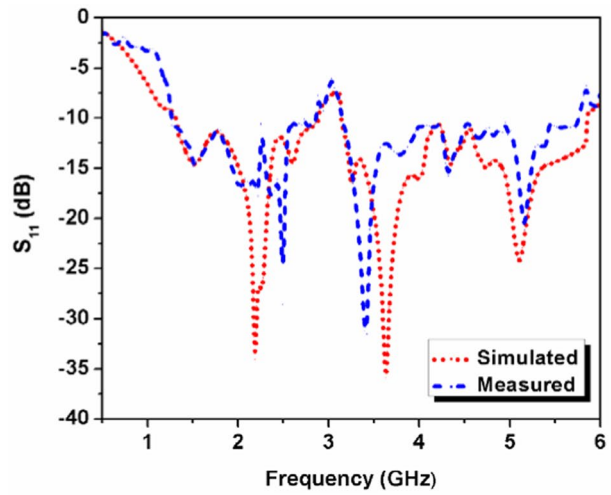

(a)
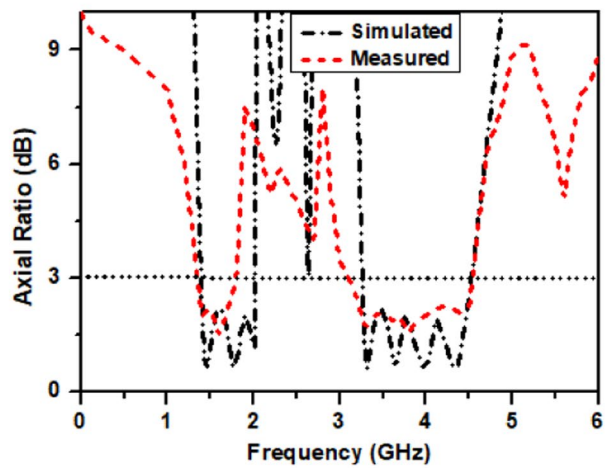
(b)

broad bandwidth due to the CPW feed, and is easier to unite with RF circuits due to its single metallic layer configuration.

- Unlike previous antenna configurations, which depend on complicated patch and ground planes, the proposed antenna employs slots and stub elements.
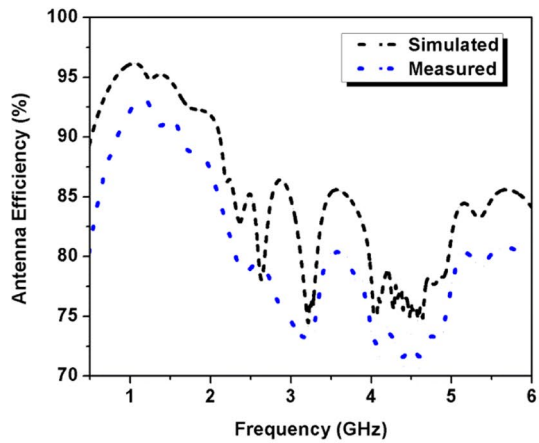
Fig. 11 Simulated and measured results of the EBG-based CPW-fed monopole antenna: **a** gain, **b** gain with additional strips/stubs, **c** antenna efficiency
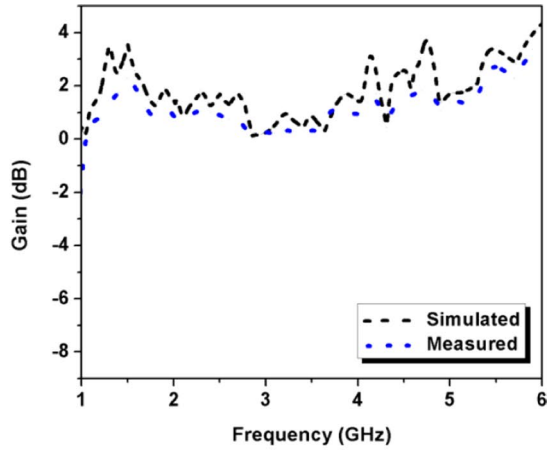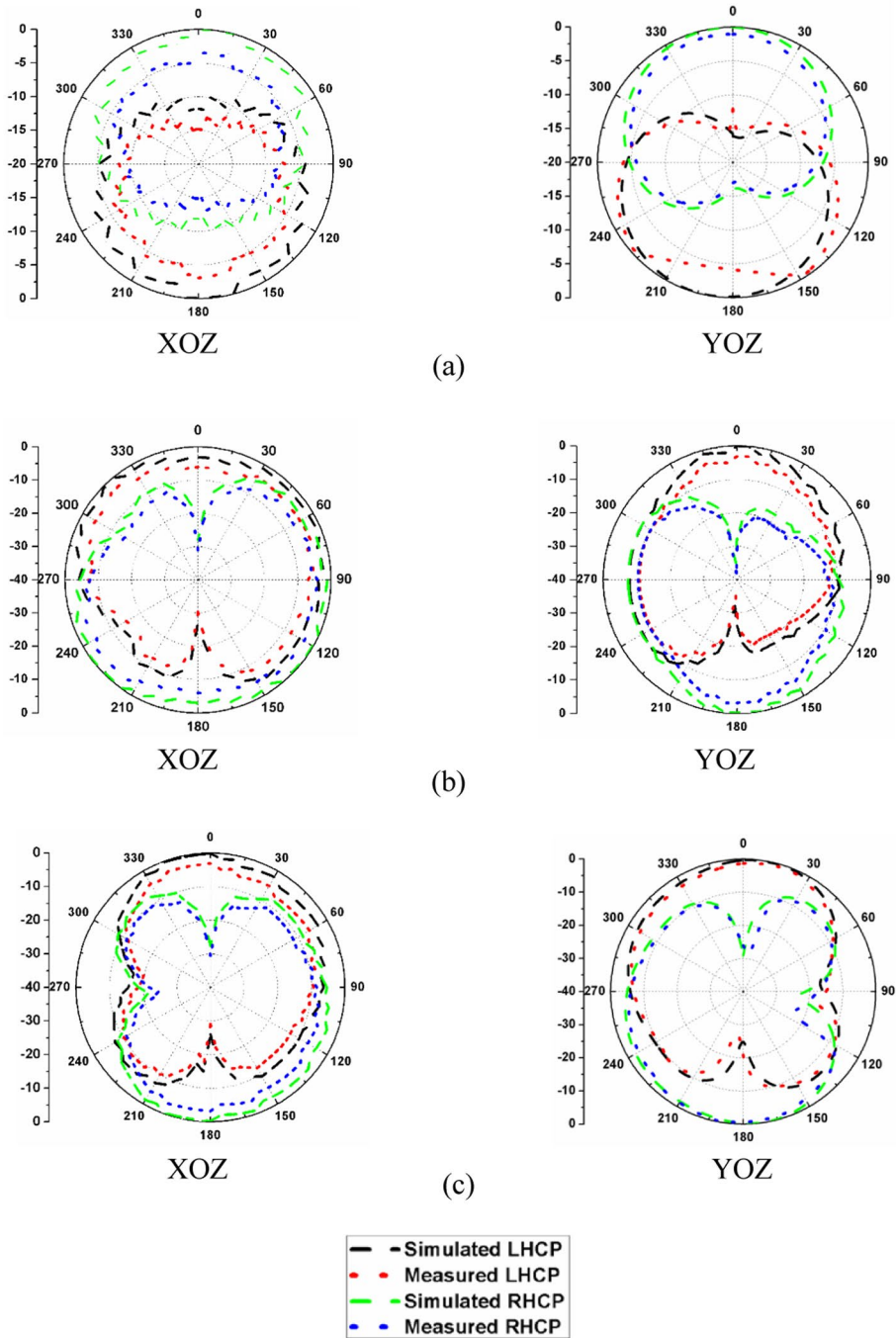

(a)
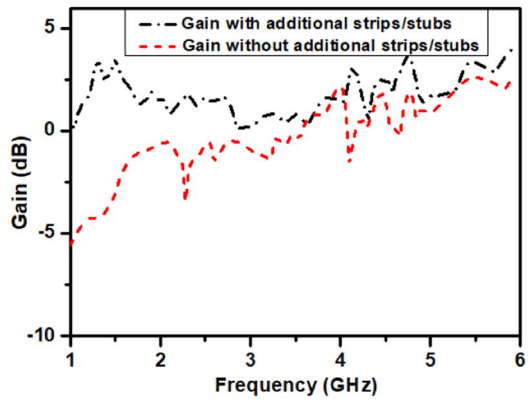
(b)

(c)

Fig. 12 Simulated and measured radiation patterns of the proposed antenna in various planes at **a** 1.45 GHz, **b** 3.63 GHz, **c** 4.34 GHz

Table 3 Comparison of the proposed EBG-based CPW-fed circularly polarized monopole antenna with other EBG-based antennas

Refs.	Antenna volume (mm×mm×mm)	Impedance bandwidth (GHz)/%	ARBW (GHz)/(%)	No. of bands	No. of layers	No. of unit cells	Presence of vias	Peak efficiency (%)	Substrate used
[7]	76×52×4	(2.81–3.43)/19.9	(2.81–3.43)/19.9	Single	Single	9	Yes	93	–
[8]	100×100×6.1	(3.25–4.14)/24	(3.45–3.65)/5.6	Single	Double	54	No	–	RT/Duroid 6002
[9]	100×100×6	(2.08–2.4)/14	(2.179–2.42)/10.6	Single	Double	16	No	–	Double special reactive impedance
[10]	39×40×4.8	(4.52–7.52)/48.6	(5.4–6.63)/20.4	Single	Double	24	No	92	Double rogers RT/ Duroid 5880
[11]	70×48×2.5	1.34, 1.91, 2.38	(2.375–2.4)/1	Single	Double	25	Yes	90	Double FR-4 epoxy
[12]	197×197×3	(2.49–2.52)/1.12	(2.51–2.56)/1.9	Single	Single	6	No	–	Special FSS
[13]	34.5×28×4	(4.20–5.90)/33.7	4.90–5.90/16.5	Single	Double	12	No	–	Double FR-4 epoxy
[14]	30×30×3.2	(2.82–4)/34.6	(3.135–3.354)/6.8	Single	Double	4	No	–	Double FR-4 epoxy
[15]	81×81×4	(2.28–2.64)/14.63	–	Single	Double	9	No	75%	Wool felt, Nora Dell-CR fabric
[16]	30×30×3.2	(5.02–7.3)/37	(5.24–5.56)/5.9	Single	Double	9	No	–	Double FR-4 epoxy
[17]	45×90×1.6	(5.51–5.68)/3.03	–	Single	Single	8	No	–	FR-4 epoxy
[18]	68×36×1.6	(5.8–6.1)/5.04	–	Single	Single	10	Yes	95.4	FR-4 epoxy
[19]	280×80×10.124	(2.67–3.412)/24.4	–	Single	Triple	14	Yes	–	Rogers Ultralam 2000, Teflon
[20]	46×27.2×1.6	(3.6–17.9)/133	–	Single	Single	16	No	96.7	FR-4 epoxy
[21]	109.5×109.5×3.4	(2.349–2.477)/5.3	(2.4269–2.477)/1.23	Single	Double	81	Yes	–	Double FR-4 epoxy
[22]	40×60×7	(2.4–2.4835)/3.42	–	Single	Double	6	No	84	Double polydimethyl-siloxane (PDMS)
[23]	18×18×3.2	(4.97–10.72)/73.29	(7.50–8.60)/13.66	Single	Double	7	No	–	Double FR-4 epoxy
[24]	38×37×3	(3.496–3.57)/2.09	–	Single	Double	4	No	–	Double FR-4 epoxy
[25]	85.6×68.4×15.204	(1.55–1.6)/3.17, (2.3–2.36)/2.6	(1.55–1.6)/3.17 (RHCP)	Narrow Double	Double	9	No	–	Double FR-4 epoxy

Table 3 (continued)

Refs.	Antenna volume (mm × mm × mm)	Impedance bandwidth (GHz)/%	ARBW (GHz)/(%)	No. of bands	No. of layers	No. of unit cells	Presence of vias	Peak efficiency (%)	Substrate used
This work	75×63×1.6	(1–2.9)/97.4, (3.05–5.75)/61.36	(1.35–1.9)/33.8 (RHCP), (3.1–4.45)/35.7 (LHCP)	Double	Single	2	No	96.8	Single FR-4 epoxy

5 Conclusion

An EBG metamaterial-based CPW-fed dual circularly polarized monopole antenna is presented. The measured results show that the proposed antenna features impedance bandwidth of 97.4% (1–2.9 GHz) in the first band covering ISM (2.4–2.4835 GHz), Wi-MAX (2.5–2.69 GHz), and WLAN (2.4–2.48 GHz) applications. The impedance bandwidth in the second band is 61.36% (3.05–5.75 GHz), which covers Wi-MAX (3.4–3.69 GHz) and WLAN (5.15–5.35 GHz) bands. In addition, the proposed antenna offers dual circular polarization with ARBW of 33.8% (1.35–1.9 GHz, RHCP) and 37.9% (3.1–4.55 GHz, LHCP). The designed antenna could be suitable for GPS (1.26–1.3 GHz), amateur satellite uplink (1.26–1.27 GHz), satellite radio (2.32–2.36 GHz), multimedia broadcasting (2.6 GHz), Bluetooth (2.4–2.48 GHz), WLAN (2.41–2.48 GHz, 5.15–5.25 GHz, 5.25–5.35 GHz), Wi-MAX (2.5–2.69 GHz), and personal digital cellular applications (1.429–1.441 GHz, 1.453–1.465 G Hz, 1.477–1.489 GHz, 1.502–1.513 GHz).

Data Availability Data will be made available on reasonable request.

Code Availability Not applicable.

Declarations

Conflict of interest The authors declare that they have no conflict of interest.

References

1. Yablonovitch, E. (1987). Inhibited spontaneous emission in solid state physics electronics. *Physical Review Letters, 58*(20), 2059–2062.
2. Wang, Q., Li, P., Rocca, P., Li, R., Tan, G., Hu, N., & Xu, W. (2023). Interval-based tolerance analysis method for petal reflector antenna with random surface and deployment errors. *IEEE Transactions on Antennas and Propagation, 71*(11), 8556–8569.
3. Smyth, B., Barth, S., & Iyer, A. K. (2016). Dual-band microstrip patch antenna using integrated uniplanar metamaterial-based EBGs. *IEEE Transactions on Antennas and Propagation, 64*(12), 5046–5053.
4. Liang, J., & Yang, H. D. (2007). Radiation characteristics of a microstrip patch over an electromagnetic bandgap surface. *IEEE Transactions on Antennas and Propagation, 55*(6), 1691–1697.
5. Afzal, M. U., Esselle, K. P., & Zeb, B. A. (2015). Dielectric phase-correcting structures for electromagnetic band gap resonator antennas. *IEEE Transactions on Antennas and Propagation, 63*(8), 3390–3399.
6. Al-Hasan, M. J., Denidni, T. A., & Sebak, A. R. (2015). Millimeter-wave compact EBG structure for mutual coupling reduction applications. *IEEE Transactions on Antennas and Propagation, 63*(2), 823–828.
7. Yang, F., & Rahmat-Samii, Y. (2004). Polarization-dependent electromagnetic band gap (PDEBG) structures: Designs and applications. *Microwave and Optical Technology Letters, 41*(6), 439–444.
8. Yang, F., & Rahmat-Samii, Y. (2005). A low profile single dipole antenna radiating circularly polarized waves. *IEEE Transactions on Antennas and Propagation, 53*(9), 3083–3086.
9. Bernard, L., Chertier, G., & Sauleau, R. (2011). Wideband circularly polarized patch antennas on reactive impedance substrates. *IEEE Antennas Wireless Propagation Letter, 10*, 1015–1018.

10. Nakamura, T., & Fukusako, T. (2011). Broadband design of circularly polarized microstrip patch antenna using artificial ground structure with rectangular unit cells. *IEEE Transactions on Antennas and Propagation, 59*(6), 2103–2110.

11. Cao, W., Zhang, B., Liu, A., Yu, T., Guo, D., & Pan, X. (2012). Multi-frequency and dual-mode patch antenna based on electromagnetic band-gap (EBG) structure. *IEEE Transactions on Antennas and Propagation, 60*(12), 6007–6012.

12. Muhammad, S. A., Sauleau, R., Le Coq, L., & Legay, H. (2011). Self-generation of circular polarization using compact Fabry-Perot cavity antennas. *IEEE Antennas Wireless Propagation Letters, 10*, 907–910.

13. Wu, Z., Li, L., Li, Y., & Chen, X. (2015). Metasurface superstrate antenna with wideband circular polarization for satellite communication application. *IEEE Antennas and Wireless Propagation Letters, 17*(15), 374–377.

14. Verma, A., Singh, A. K., Srivastava, N., Patil, S., & Kanaujia, B. K. (2020). Slot loaded EBG-based metasurface for performance improvement of circularly polarized antenna for WiMAX applications. *International Journal of Microwave and Wireless Technologies., 12*(3), 212–220.

15. Gao, G. P., Hu, B., Wang, S. F., & Yang, C. (2018). Wearable circular ring slot antenna with EBG structure for wireless body area network. *IEEE Antennas Wireless Propag. Lett., 17*(3), 434–437.

16. Verma, A., Singh, A. K., Srivastava, N., Patil, S., & Kanaujia, B. K. (2021). Performance enhancement of circularly polarized patch antenna using slotted circular EBG-based metasurface. *Frequenz, 75*(1–2), 35–47.

17. Mohamadzade, B., & Afsahi, M. (2017). Mutual coupling reduction and gain enhancement in patch array antenna using a planar compact electromagnetic bandgap structure. *IET Microwaves & Antennas Propagation, 11*(12), 1719–1725.

18. Naderi, M., Zarrabi, F. B., Jafari, F. S., & Ebrahimi, S. (2018). Fractal EBG structure for shielding and reducing the mutual coupling in microstrip patch antenna array. *AEU–International Journal of Electronics and Communications, 93*, 261–267.

19. Jam, S., & Simrun, M. (2018). Performance enhancement of a compact wideband patch antenna array using EBG structures. *AEU–International Journal of Electronics and Communications, 89*, 42–55.

20. Dabas, T., Gangwar, D., Kanaujia, B. K., & Gautam, A. K. (2018). Mutual coupling reduction between elements of UWB MIMO antenna using small size uniplanar EBG exhibiting multiple stop bands. *AEU–International Journal of Electronics and Communications, 93*, 32–38.

21. Ke Wang, Z., Yuan, B., Zhang, X. H., & Luo, G. Q. (2017). An axial-ratio beam-width enhancement of patch-slot antenna based on EBG. *Microwave and Optical Technology Letters, 59*(3), 493–497.

22. Gao, G., Zhang, R., Yang, C., Meng, H., Geng, W., & Hu, B. (2019). Microstrip monopole antenna with a novel UC-EBG for 2.4 GHz WBAN applications. *IET Microwaves, Antennas & Propagation, 13*(13), 2319–2323.

23. Verma, A., Patil, S., Singh, A. K., & Pandey, A. K. (2023). Notched circular EBG based circularly polarized antenna for performance enhancement. *Journal of Microwaves, Optoelectronics and Electromagnetic Applications., 13*(22), 47–62.

24. Raut, H., Kingsly, S., Subbaraj, S., & Malekar, R. (2024). EBG-based slotted T-shaped antenna for sub-6 GHz 5G application. *International Journal of Electronics Letters, 5*, 1–3.

25. Khan, S. F., Khan, B. M., & Rasool Khan, T. M. (2024). Low profile high gain RHCP antenna for L-Band and S-Band using rectangular ring metasurface with backlobe suppression. *PLoS ONE, 19*(2), e0297957.

26. Veselago, V. G. (1968). The electrodynamics of substances with simultaneously negative values of ε and μ. *Soviet Physics Uspekhi, 10*(4), 509–514.

27. Shelby, R. A., Smith, D. R., & Schultz, S. (2001). Experimental verification of a negative index of refraction. *Science, 292*(5514), 77–79.

28. Huang, X., Zhou, L., Xu, J., Zhang, X. Y., & Mao, J. (2022). BCB-based thin-film Ka-band quarter-mode siw packaged filters with ultrawide stopband and independently controlled TZs. *IEEE Transactions on Microwave Theory and Techniques, 70*(10), 4389–4398.

29. Smyth, B. P., Iyer, A. K. (2020). Embedded MTM-EBGs in patch antenna for simultaneously dual-band and dual-polarized operation. In *2020 14th European Conference on Antennas and Propagation (EuCAP)*, (pp. 1–4). IEEE.

30. Barth, S., & Iyer, A. K. (2016). A miniaturized uniplanar metamaterial-based EBG for parallel-plate mode suppression. *IEEE Transactions on Microwave Theory and Techniques., 64*(4), 1176–1185.

31. Smyth, B. P., Iyer, A. K. (2018). Compact tri-band microstrip stub filter using embedded MTM-EBGs. In *2018 IEEE International Symposium on Antennas and Propagation & USNC/URSI National Radio Science Meeting*, (pp. 163–164). IEEE.

32. Saha, D., Saha, C. (2022). MTM-EBG Loaded Circular Patch Antenna for ISM Band Applications. In *2022 IEEE Microwaves, Antennas, and Propagation Conference (MAPCON)*, (pp. 1788–1791). IEEE.

33. Barth, S., Iyer, A. K. (2017). A low-profile dual-band circular patch antenna for GPS using metamaterial-based EBGs. In *2017 IEEE International Symposium on Antennas and Propagation & USNC/URSI National Radio Science Meeting*, (pp. 1727–1728). IEEE.

34. Feng, Y., Xu, K., Niu, Z., Zhang, B., Liu, L., & Fan, Y. (2024). Ka-band waveguide bandpass filters using double-layer grounded spoof surface Plasmon Polaritons. *IEEE Transactions on Microwave Theory and Techniques*. https://doi.org/10.1109/TMTT.2024.3373504

35. Yang, F., & Rahmat-Samii, Y. (2003). Microstrip antennas integrated with electromagnetic bandgap (EBG) structures: A low mutual coupling design for array applications. *IEEE Transactions on Antennas and Propagation, 51*(10), 2936–2946.

36. Huang, X., Zhou, L., Yuan, Y., Qiu, L., & Mao, J. (2019). Quintuple-mode W-band packaged filter based on a modified quarter-mode substrate-integrated waveguide cavity. *IEEE Transactions on Components, Packaging and Manufacturing Technology, 9*(11), 2237–2247.

37. Sievenpiper, D., Zhang, L., Broas, R. F., Alexopolous, N. G., & Yablonovitch, E. (1999). High-impedance electromagnetic surfaces with a forbidden frequency band. *IEEE Transactions on Microwave Theory and Techniques, 47*(11), 2059–2074.

38. Yang, F., & Sami, Y. R. (2003). The effects of an electromagnetic bandgap (EBG) structure on two element microstrip patch antenna array. *IEEE Transactions Antennas and Propagation, 51*(10), 2936–2946.

39. Abdulhameed, M. K., Isa, M. M., Zakaria, Z., Mohsin, M. K., & Attiah, M. L. (2018). Mushroom-like EBG to improve patch antenna performance for C-band satellite application. *International Journal of Electrical and Computer Engineering., 8*(5), 3875.

40. Zheng, Q. R., Fu, Y. Q., & Yuan, N. C. (2008). A novel compact spiral electromagnetic band-gap (EBG) structure. *IEEE Transactions on Antennas and Propagation, 56*(6), 1656–1660.

41. Cheype, C., Serier, C., Thevenot, M., Monediere, T., Reineix, A., & Jecko, B. (2002). An electromagnetic bandgap resonator antenna. *IEEE Transactions on Antennas and Propagation, 50*(9), 1285–1290.

42. Samson, D. R. (2021). Planar SIW cavity-backed antenna loaded with slots for multiband operations. *Applied Physics A, 127*(6), 454.

43. Daniel, R. S. (2021). A CPW-fed rectangular nested loop antenna for penta band wireless applications. *AEU-International Journal of Electronics and Communications., 1*(139), 153891.

44. Wu, J., Ren, X., Li, Z., & Yin, Y. Z. (2013). Modified square slot antennas for broadband circular polarization. *Progress In Electromagnetics Research C., 38*, 1–4.

45. Saini, R. K., Dwari, S., & Mandal, M. K. (2017). CPW-fed dual-band dual-sense circularly polarized monopole antenna. *IEEE Antennas and Wireless Propagation Letters, 13*(16), 2497–2500.

46. Hussain, N., Abbas, A., Park, S. M., Park, S. G., & Kim, N. (2022). A compact tri-band Antenna based on inverted-L stubs for smart devices. *Computers, Materials & Continua, 70*(2), 3321–3331.

47. Huang, X., Zhang, X., Zhou, L., Xu, J., & Mao, J. (2023). Low-loss self-packaged Ka-band LTCC filter using artificial multimode SIW resonator. *IEEE Transactions on Circuits and Systems II: Express Briefs, 70*(2), 451–455.

48. Tran, H. H., & Nguyen-Trong, N. (2021). Performance enhancement of MIMO patch antenna using parasitic elements. *IEEE Access, 10*(9), 30011–30016.

49. Gao, N., Liu, J., Deng, J., Chen, D., Huang, Q., & Pan, G. (2024). Design and performance of ultra-broadband composite meta-absorber in the 200Hz-20kHz range. *Journal of Sound and Vibration, 574*, 118229.

50. Iqbal, J., Illahi, U., Yasin, M. N., Albreem, M. A., & Akbar, M. F. (2022). Bandwidth enhancement by using parasitic patch on dielectric resonator antenna for sub-6 GHz 5G NR bands application. *Alexandria Engineering Journal., 61*(6), 5021–5032.

51. Sim, C. Y. (2008). Dual band CPW-fed monopole antenna with asymmetrical ground plane for bandwidth enhancement. *Microwave and Optical Technology Letters, 50*(11), 3001–3004.

52. Liu, W. C., & Liu, H. J. (2006). Compact triple-band slotted monopole antenna with asymmetrical CPW grounds. *Electronics Letters, 42*(15), 840–842.

53. Babu, N. S., Ansari, A. Q., Gangwar, D., Kanaujia, B. K., Kumar, S., & Gupta, S. K. (2023). Dual-band circularly-polarized EBG-based antenna for Wi-MAX/WLAN/ISM band applications. *Wireless Personal Communications, 128*(1), 231–248.

54. Ding, K., Guo, Y. X., & Gao, C. (2016). CPW-fed wideband circularly polarized printed monopole antenna with open loop and asymmetric ground plane. *IEEE Antennas and Wireless Propagation Letters, 7*(16), 833–836.

55. Mousavi, P., Miners, B., & Basir, O. (2010). Wideband L-shaped circular polarized monopole slot antenna. *IEEE Antennas and Wireless Propagation Letters, 12*(9), 822–825.

56. Alam, M. M., Azim, R., Sobahi, N. M., Khan, A. I., & Islam, M. T. (2022). A dual-band CPW-fed miniature planar antenna for S-, C-, WiMAX, WLAN, UWB, and X-band applications. *Scientific Reports, 12*(1), 7584.

Nallagundla Suresh Babu received the Bachelor degree in Electronics and Communication Engineering (ECE) from Nagarjuna University, Guntur, India, in 1996, and Master's degree in Laser and Electro-Optical Engineering from Anna University, Chennai, India, in 1998. He is currently pursuing his Ph.D. degree in Electrical Engineering from the Faculty of Engineering and Technology, Jamia Millia Islamia, New Delhi, India. He had worked as a Lecturer in the ECE Department, St. Peter's Engineering College, Chennai, India, from June, 1998 to September, 2000. He is working as a Senior Faculty Member and Officiating HoD in the Department of ECE, Meera Bai Institute of Technology, Directorate of Training & Technical Education, Govt. of NCT. of Delhi, India. His current research interests focus on microstrip patch antennas, circularly polarized antennas, wideband, and multiband antennas.

Abdul Quaiyum Ansari is working as a Professor in the Department of Electrical Engineering, Faculty of Engineering and Technology, Jamia Millia Islamia (JMI), New Delhi, India. He has more than 34 years of teaching experience. He had served as an Associate Professor (on extra-ordinary leave from JMI) in the College of Computer Science, King Khalid University, Kingdom of Saudi Arabia. He had supervised many M.Tech. scholars and 14 Ph.D. research scholars so far. Prof. Ansari had published two patents and had completed three projects sponsored by UGC and AICTE. He has been credited to publish more than 190 research papers with more than 1000 citations and h-index of 15 in several peer-reviewed journals and conferences. His areas of research are computer networking and data communication, image processing, networks on chip, soft computing, and microstrip antennas.

Deepak Gangwar received the B.Tech. degree from Uttar Pradesh Technical University, Lucknow, India, in 2008, and M.Tech. degree from Guru Gobind Singh Indraprastha University, Delhi, India in 2011. He received the Ph.D. degree in Electronics Engineering from the Indian Institute of Technology (ISM), Dhanbad, India. Currently, he is working as an Associate Professor in the Mahatma Jyotiba Phule Rohilkhand University, Bareilly, India. His research interest includes metamaterial-based antennas, ultra-wideband antennas, metamaterial filters, frequency selective surface, metasurface, and RCS reduction.

Binod Kumar Kanaujia received the B.Tech. degree in Electronics Engineering from the Kamla Nehru Institute of Technology, Sultanpur, India, in 1994, and the M.Tech. and Ph.D. degrees from the Department of Electronics Engineering, Indian Institute of Technology (Banaras Hindu University), Varanasi, India, in 1998 and 2004, respectively. He has been a Professor and the Dean of the School of Computational and Integrative Sciences, Jawaharlal Nehru University, New Delhi, India, since August 2016, and the Director (Deputation) of the Dr. B. R. Ambedkar National Institute of Technology Jalandhar, Jalandhar, India, since February 2022. Prior to his career in academics, he was an Executive Engineer with the Research & Development Division, M/s Uptron India Ltd. He has been credited with publishing more than 400 research papers, three books, 11 book chapters, and ten patents with more than 4600 citations with an H-index of 32 in peer-reviewed journals and conferences. He had supervised 50 M.Tech. and 35 Ph.D. research scholars in the field of microwave engineering. His research interests include the design and modeling of microstrip antenna, dielectric resonator antenna, left-handed metamaterial microstrip antenna, shorted microstrip antenna, ultra-wideband antennas, and reconfigurable, and circular polarized antennas for wireless communication. He is a member of several academic and professional bodies, such as the Indian Society for Technical Education, and a fellow of the Institution of Engineers, India, and the Institute of Electronics and Telecommunication Engineers of India. He has successfully executed six research projects with three ongoing projects sponsored by several agencies of the Government of India, such as DRDO, DST, DBT, SERB, AICTE, and ISRO. He is an Associate Editor of *IEEE Access* and an Editor of *AEU-International Journal of Electronics and Communication* (Elsevier) and *IETE Technical Review* (Taylor and Francis).

Sachin Kumar received the B.Tech. degree in Electronics and Communication engineering from Uttar Pradesh Technical University, Lucknow, India, in 2009, and the M.Tech. and Ph.D. degrees in Digital Communication and in RF and Microwave Engineering from the Netaji Subhas University of Technology (East Campus), Delhi, India, in 2011 and 2016, respectively. He was a Postdoctoral Research Fellow with the College of IT Engineering, Kyungpook National University, South Korea, from 2018 to 2021. He is currently the Deputy Dean (R&D) and an Associate Professor with the Department of Electronics and Communication Engineering, Galgotias College of Engineering and Technology, Greater Noida, India. He has published two books, 12 book chapters, five patents, 140 research articles in SCI journals, and over 50 papers in international conferences; and his articles have been cited over 2700 times with an H-index of 29. Dr. Kumar is a fellow of the Institute of Electronics and Telecommunication Engineers, India, a Life Member of Indian Society for Technical Education, and a member of Korean Institute of Electromagnetic Engineering and Science. He is

also a frequent reviewer for more than 60 scientific journals and book publishers. He has given several invited talks at prestigious institutions and serves as the session chair, an organizer, and a member of the technical program committee for various national/international conferences, summits, and workshops. His name was featured in the list of ''World's Top 2% Scientists,'' in 2022, 2021, and 2020, database released by Stanford University, USA, and Elsevier. He was a recipient of the Teaching-cum-Research Fellowship from the Government of NCT of Delhi, India, and the Brain Korea 21 Plus Research Fellowship from the National Research Foundation of South Korea. He is an Associate Editor of *Frontiers in Antennas and Propagation* and *Franklin Open*; an Advisory Board Member of *Measurement*; an Editorial Board Member of *Current Chinese Science, Journal of High-Frequency Communication Technologies, Transactions on Electromagnetic Spectrum*, and *Wearable Technology*; and a Guest Editor of the *International Journal of Antennas and Propagation, Electronics*, and *Micromachines*.

Surendra Kumar Gupta received the Bachelor degree in Electronics & Telecommunication Engineering from the Institution of Engineers (India), Kolkata, India, in 1994, and Masters of Engineering in Digital Systems from Motilal Nehru Regional Engineering College, University of Allahabad, India, in 1999. He received the Ph.D. degree in the field of Microstrip Antennas from Uttarakhand Technical University, Dehradun, India, in 2015. He was associated as Quality Assurance Services (Avionics)–Inspector with Air Force Station, Kanpur, India, from July 1995 to January 2000. He worked as a Lecturer and Department Coordinator of the Electronics and Communication Engineering at Moradabad Institute of Technology, Moradabad, India, from February 2000–June 2002. Since July 2002, he is a Senior Faculty Member in the Department of Electronics Engineering, Ambedkar Institute of Technology, Government of Delhi, India. He has authored/co-authored more than 20 research papers in various international journals and conferences. His research interest includes computer-aided design, wireless communication, and microstrip antennas. He is a reviewer for several journals of international/national repute. He is a life member of the Indian Society of Technical Education, India and Associate Member of Institute of Engineers, India.